ELSEVIER

Heat transfer to non-Newtonian fluids in laminar flow through rectangular ducts

Mônica F. Naccache and Paulo R. Souza Mendes
Department of Mechanical Engineering, Pontifícia Universidade Católica, Rio de Janeiro, Brazil

Heat transfer to non-newtonian fluids flowing laminarly through rectangular ducts is examined. The conservation equations of mass, momentum, and energy are solved numerically with the aid of a finite volume technique. The viscoelastic behavior of the fluid is represented by the Criminale–Ericksen–Filbey (CEF) constitutive equation. Secondary flows occur due to the elastic behavior of the fluid, and, consequently, heat transfer is strongly enhanced. It is observed that shear thinning yields negligible heat transfer enhancement effect, when compared with the secondary flow effect. Maximum heat transfer is shown to occur for some combinations of parameters. Thus, there are optimal combinations of aspect ratio and Reynolds numbers, which depend on the fluid's mechanical behavior. This result can be usefully explored in thermal designs of certain industrial processes.

Keywords: flow of viscoelastic liquids; forced convection through rectangular ducts; Criminale–Erickson–Filbey (CEF) equation

Introduction

Flows of non-Newtonian fluids through ducts of noncircular cross section have been analyzed numerically and experimentally by a number of authors. Townsend et al. (1976) studied numerically and experimentally the flow through square ducts of a viscoelastic liquid and observed the existence of secondary flows in the cross-section plane. These secondary flows are in the form of eight vortices arranged symmetrically. Gervang and Larsen (1991) have recently analyzed this problem numerically for other aspect ratios and also observed the presence of vortices. They noted that, as the aspect ratio is increased, the vortices become different in shape, strength, and size.

The heat transfer problem has also been investigated for this flow. For purely viscous non-Newtonian fluids, Chandrupatla and Sastri (1977) and Gringrich et al. (1992) have shown that for shear thinning fluids, heat transfer is more intense than for Newtonian fluids. For shear thickening fluids, the opposite trend is observed.

For viscoelastic fluids, heat transfer rates are typically larger than for Newtonian fluids. Mena et al. (1978) investigated flows of polymeric solutions in triangular and rectangular ducts, while Naccache and Souza Mendes (1992) analyzed numerically fully developed flows through rectangular ducts of different aspect ratios. Hartnett and Kostic (1985) studied experimentally the thermal entrance region of rectangular ducts and compared the entrance region flow of viscoelastic and Newtonian fluids. Their results suggested that secondary flows are responsible for the heat transfer enhancement observed. However, no flow visualization results have been reported. Dunwoody and Hamill (1980) analyzed both the dynamic and the thermal problems numerically, using as constitutive equation the third-order fluid model. Hartnett (1992) and Kostic (1994) offer comprehensive surveys on the subject.

A common observation reported in these papers is that, for laminar flows through ducts of noncircular cross sections, heat transfer phenomena involving non-Newtonian fluids are significantly different from their Newtonian counterparts. Two distinct effects cause these differences; namely, (1) the viscosity dependence on shear rate (shear thinning or thickening fluids); and (2) secondary flows caused by elastic effects.

In general, viscoelastic fluids show both viscosity dependence on shear rate and elastic behavior. To describe mathematically the mechanical behavior of this kind of fluid, it is necessary to use relatively complex constitutive relations, such as retarded motion expansions, differential or integral models (Bird et al. 1987). The Generalized Newtonian Liquid model, widely used for representing the viscosity dependence on shear rate, is not capable of predicting elastic mechanical behavior.

Gao and Hartnett (1996) studied this problem with the aid of the Reiner–Rivlin model, which is capable of predicting nonzero second normal stress coefficients. This model, however, predicts a null first normal stress coefficient, which is shown in the present paper to have significant effects in the secondary flow strength and, hence, in heat transfer.

In this work the Criminale–Ericksen–Filbey (CEF) equation is employed as constitutive equations. It is similar to a second-order fluid, except that the coefficients are allowed to be functions of $\dot{\gamma}$, the deformation rate. It is an attractive choice for this problem, because it is perhaps the simplest constitutive equation that can predict shear thinning (or thickening) together with nonzero first and second normal stress differences in steady simple shear flows. (Steady simple shear flows have a velocity field of the form $\mathbf{v} = \dot{\gamma} y \hat{\mathbf{e}}_x$, where $\dot{\gamma}$ is a constant, in some x, y, z

Address reprint requests to Prof. R. S. Souza Mendes, Department of Mechanical Engineering, Pontifícia Universidade Católica, Rio de Janeiro, RJ 22453-900 Brazil.

Received 20 December 1995; accepted 7 May 1996

Int. J. Heat and Fluid Flow 17: 613–620, 1996

655 Avenue of the Americas, New York, NY 10010

0142-727X/96/$15.00
PII S0142-727X(96)00062-7

Cartesian coordinate system.) The driving force that causes secondary flows in noncircular ducts is known to be related to the mechanism that generates second normal stress differences in steady simple shear flows (e.g., Townsend et al. 1976).

This paper reports a numerical investigation on heat transfer to viscoelastic liquids flowing in a rectangular duct. Among other conclusions, it is shown that the secondary flow is, indeed, the enhancing mechanism for heat transfer and that the Nusselt number depends on the duct aspect ratio in a different fashion, as compared to the trends observed for Newtonian fluids. More details of the research reported here can be found in Naccache (1993).

Analysis

The problem under study is depicted in Figure 1. The geometry consists of a duct of rectangular cross section, with aspect ratio $\alpha = B/H$. The side walls are adiabatic, while the top and bottom ones are uniformly heated.

The flow is assumed to be laminar and steady, and the compressibility of the fluid is neglected. Neither natural convection nor temperature-dependent properties are considered in the present analysis.

Governing equations

For the situation described above, the conservation equations are:

$$\operatorname{div}\mathbf{v} = 0 \tag{1}$$

$$\rho \operatorname{div}(\mathbf{vv}) = -\operatorname{grad} p + \operatorname{div}\boldsymbol{\tau} + \rho\mathbf{g} \tag{2}$$

$$\rho c\mathbf{v}\cdot\operatorname{grad} T = k\nabla^2 T \tag{3}$$

where $\mathbf{v}$ is the velocity vector field, ρ the mass density, c the specific heat, k the thermal conductivity, T the temperature, p the pressure, and $\mathbf{g}$ the acceleration due to gravity. The extra-stress tensor $\boldsymbol{\tau}$ is the part of the stress tensor that vanishes when there is no motion other than rigid-body translation and rotation and is a function of the flow kinematics. For viscoelastic fluid behavior, it is often convenient to decompose $\boldsymbol{\tau}$ into two terms; namely, a Newtonian-like term and a polymeric term $\boldsymbol{\tau}^P$. The latter depends on the constitutive equation chosen.

$$\boldsymbol{\tau} = \eta(\dot{\gamma})\dot{\boldsymbol{\gamma}} + \boldsymbol{\tau}^P \tag{4}$$

In the above equation, $\dot{\boldsymbol{\gamma}} = \operatorname{grad}\mathbf{v} + (\operatorname{grad}\mathbf{v})^T$ is the rate-of-deformation tensor. The scalar rate of deformation $\dot{\gamma}$ is defined as $\dot{\gamma} \equiv \sqrt{(1/2)\operatorname{tr}\dot{\boldsymbol{\gamma}}^2}$, and $\eta(\dot{\gamma})$ is the viscosity function.

Notation

a	parameter of the Carreau–Yasuda equation, Equation 16
B	duct width, m
c	specific heat, J/kg K
D_h	duct hydraulic diameter, m
De_1	first Deborah number
De_2	second Deborah number
$\hat{\mathbf{e}}_x, \hat{\mathbf{e}}_y, \hat{\mathbf{e}}_z$	unit vectors in the x, y, z directions, respectively, Figure 1
f	friction factor, $\equiv (2(\partial p/\partial z)D_h)/(\rho\overline{w}^2)$
g	magnitude of the acceleration due to gravity, m/s^2
$\mathbf{g}$	acceleration due to gravity, $= -g\hat{\mathbf{e}}_y$, m/s^2
H	duct height, m
k	thermal conductivity, W/mK
n	power-law exponent of the Carreau–Yasuda equation, Equation 16
p	pressure, PA
P	dimensionless pressure
Pr	Prandtl number
q_w	wall heat flux, W/m^2
$\overline{q}_w$	mean wall heat flux, W/m^2
Re	Reynolds number
T	temperature field, °C
T_b	bulk temperature, °C
T_w	wall temperature, °C
$\overline{T}_w$	mean wall temperature, °C
u	x-component of velocity, m/s
U	dimensionless x-component of velocity
v	y-component of velocity, m/s
v_c	characteristic flow velocity, m/s
$\mathbf{v}$	velocity vector field, m/s
V	dimensionless y-component of velocity
x	horizontal cross-wise coordinate, m
X	dimensionless horizontal cross-wise coordinate
y	vertical coordinate, m
Y	dimensionless vertical coordinate
w	z-component of velocity (axial velocity), m/s
$\overline{w}$	mean axial velocity, m/s
W	dimensionless axial velocity
$\overline{W}$	dimensionless mean axial velocity
We	Weissenberg number
z	axial coordinate, m
Z	dimensionless axial coordinate

Greek

α	duct aspect ratio, $\equiv B/H$
$\dot{\gamma}$	deformation rate, $\equiv \sqrt{\frac{1}{2}\operatorname{tr}\dot{\boldsymbol{\gamma}}^2}$, (s^{-1})
$\dot{\gamma}^*$	dimensionless deformation rate, $\equiv \dot{\gamma}/\dot{\gamma}_c$
$\dot{\gamma}_c$	characteristic deformation rate, s^{-1}
$\dot{\boldsymbol{\gamma}}$	rate-of-deformation tensor, s^{-1}
$\boldsymbol{\gamma}_{[2]}$	second rate-of-deformation tensor, s^{-2}
Δ_ψ	stream function difference, $\equiv \psi_{\max} - \psi_{\min}$, kg/ms
η	viscosity function, kg/ms
η_c	characteristic viscosity, kg/ms
η_0	zero-shear rate viscosity, kg/ms
η_∞	infinite-shear viscosity, kg/ms
η^*	dimensionless viscosity
η_0^*	dimensionless zero-shear rate viscosity
η_∞^*	dimensionless infinite-shear rate viscosity
θ	dimensionless temperature
λ	characteristic time of fluid, s
$\boldsymbol{\tau}$	extra-stress tensor, Pa
$\boldsymbol{\tau}^P$	polymeric part of $\boldsymbol{\tau}$, Pa
$\boldsymbol{\tau}^{P*}$	dimensionless $\boldsymbol{\tau}^P$
ψ	stream function, defined by $\partial\psi/\partial x \equiv -\rho v$; $\partial\psi/\partial y \equiv \rho u$; $\partial\psi/\partial z \equiv 0$, kg/ms
$\psi_{\max}$	maximum value of the stream function, kg/ms
$\psi_{\min}$	minimum value of the stream function, kg/ms
Ψ_1	first normal stress coefficient, Pa s^2
Ψ_2	second normal stress coefficient, Pa s^2
Ψ_1^*	dimensionless first normal stress coefficient
Ψ_2^*	dimensionless second normal stress coefficient

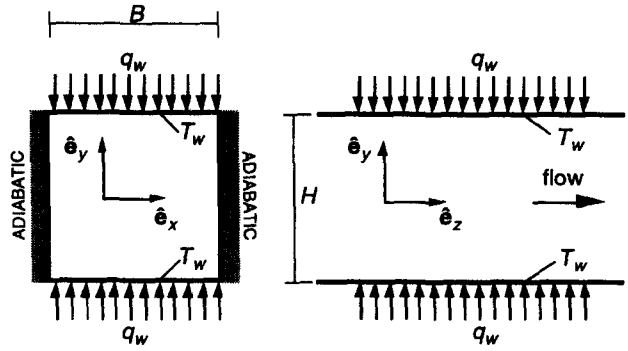

Figure 1 Schematics of the problem

For the present situation, a Cartesian coordinate system is appropriate. Thus, the velocity vector is accordingly written as $\mathbf{v} \equiv u\hat{\mathbf{e}}_x + v\hat{\mathbf{e}}_y + w\hat{\mathbf{e}}_z$, where z is the axial coordinate, and x and y are, respectively, the horizontal (transversal) and vertical coordinates.

In this work, we examine the situation of fully developed flow. Thus, velocity and dimensionless temperature profiles are the same in all cross sections along the duct length (no z-dependence). This allows the flow to be treated as two-dimensional (2-D), and the conservation equations for this situation make up a set of elliptical, nonlinear partial differential equations that can be written in the following dimensionless form:

$$U\frac{\partial U}{\partial X} + V\frac{\partial U}{\partial Y} = -\frac{\partial P}{\partial X} + \frac{1}{\mathrm{Re}}\left[\frac{\partial}{\partial X}\left(2\eta^*\frac{\partial U}{\partial X}\right) + \frac{\partial}{\partial Y}\left(\eta^*\frac{\partial U}{\partial Y} + \eta^*\frac{\partial V}{\partial X}\right)\right] + \left(\frac{\partial \tau_{xx}^{P*}}{\partial X} + \frac{\partial \tau_{xy}^{P*}}{\partial Y}\right) \tag{5}$$

$$U\frac{\partial V}{\partial X} + V\frac{\partial V}{\partial Y} = -\frac{\partial P}{\partial Y} + \frac{1}{\mathrm{Re}}\left[\frac{\partial}{\partial Y}\left(2\eta^*\frac{\partial V}{\partial Y}\right) + \frac{\partial}{\partial X}\left(\eta^*\frac{\partial V}{\partial X} + \eta^*\frac{\partial U}{\partial Y}\right)\right] + \left(\frac{\partial \tau_{xy}^{P*}}{\partial X} + \frac{\partial \tau_{yy}^{P*}}{\partial Y}\right) \tag{6}$$

$$U\frac{\partial W}{\partial X} + V\frac{\partial W}{\partial Y} = -\frac{\partial P}{\partial Z} + \frac{1}{\mathrm{Re}}\left[\frac{\partial}{\partial X}\left(\eta^*\frac{\partial W}{\partial X}\right) + \frac{\partial}{\partial Y}\left(\eta^*\frac{\partial W}{\partial Y}\right)\right] + \left(\frac{\partial \tau_{xz}^{P*}}{\partial X} + \frac{\partial \tau_{yz}^{P*}}{\partial Y}\right) \tag{7}$$

The mass and energy conservation equations, in dimensionless form, are written as

$$\frac{\partial U}{\partial X} + \frac{\partial V}{\partial Y} = 0 \tag{8}$$

$$U\frac{\partial \theta}{\partial X} + V\frac{\partial \theta}{\partial Y} = \frac{1}{\mathrm{Re}\,\mathrm{Pr}}\left[\left(\frac{\partial^2\theta}{\partial X^2} + \frac{\partial^2\theta}{\partial Y^2}\right) - \frac{4\alpha}{\alpha+1}\frac{W}{\overline{W}}\right] \tag{9}$$

The dimensionless variables appearing above are defined as:

$$X = x/D_h \qquad Y = y/D_h \qquad Z = z/D_h$$
$$U = u/v_c \qquad V = v/v_c \qquad W = w/v_c$$
$$\theta = \frac{T - T_b}{(q_w D_h/k)} \qquad \tau^{P*} = \tau^P/\rho v_c^2 \qquad P = \frac{p + \rho g y}{\rho v_c^2}$$

$$\eta^* = \eta/\eta_c \tag{10}$$

where v_c is a characteristic velocity (to be defined later), and $D_h = 2B/(\alpha + 1)$ is the hydraulic diameter. The bulk temperature T_b is evaluated as usual:

$$T_b = \frac{4}{\overline{w}BH}\int_0^{H/2}\int_0^{B/2} wT\,\mathrm{d}x\,\mathrm{d}y \tag{11}$$

The characteristic viscosity η_c is defined as

$$\eta_c \equiv \eta(\dot{\gamma}_c) \tag{12}$$

where $\dot{\gamma}_c \equiv v_c/D_h$ is the characteristic shear rate.

The Reynolds number Re and Prandtl number Pr are defined as

$$\mathrm{Re} = \frac{\rho v_c D_h}{\eta_c} \qquad \mathrm{Pr} = \frac{\eta_c c}{k} \tag{13}$$

Constitutive equation

As mentioned earlier, the CEF equation is employed to represent the mechanical fluid behavior. In this case, the extra stress tensor becomes

$$\boldsymbol{\tau} = \eta(\dot{\gamma})\dot{\boldsymbol{\gamma}} - \tfrac{1}{2}\Psi_1(\dot{\gamma})\boldsymbol{\gamma}_{[2]} + \Psi_2(\dot{\gamma})\dot{\boldsymbol{\gamma}} \tag{14}$$

where

$$\boldsymbol{\gamma}_{[2]} \equiv \frac{\mathrm{d}\dot{\boldsymbol{\gamma}}}{\mathrm{d}t} - [(\mathrm{grad}\,\mathbf{v})^T \cdot \dot{\boldsymbol{\gamma}} + \dot{\boldsymbol{\gamma}} \cdot (\mathrm{grad}\,\mathbf{v})] \tag{15}$$

is the second rate-of-deformation tensor. The operator d/dt appearing in the above definition is the material time derivative. Usually, the quantities $\eta(\dot{\gamma})$, $\Psi_1(\dot{\gamma})$, and $\Psi_2(\dot{\gamma})$ are, respectively, identified with material functions measured in steady simple shear flow; namely, the viscosity, first, and second normal stress coefficients. This is a reasonable assumption for predominantly shear flows, like the present one. The deformation rate $\dot{\gamma}$ reduces to the shear rate for steady simple shear flow.

The viscosity function $\eta(\dot{\gamma})$ is given by the Carreau–Yasuda equation:

$$\eta(\dot{\gamma}) = \eta_\infty + (\eta_0 - \eta_\infty)[1 + (\lambda\dot{\gamma})^a]^{(n-1)/a} \tag{16}$$

The first and second normal stress coefficients $\Psi_1(\dot{\gamma})$ and $\Psi_2(\dot{\gamma})$ are assumed to be constant for simplicity. Preliminary tests, performed in the course of the present research, indicated that constant and variable normal stress coefficients yield the same qualitative results for typical dependences of Ψ_1 and Ψ_2 on $\dot{\gamma}$.

It is known that typical values of Ψ_2 for polymeric liquids are in the range $-0.25\Psi_1 < \Psi_2 < -0.10\Psi_1$ (Bird et al. 1987). Thus, in the present research, the values of first and second normal stress coefficients are such that $\Psi_2 = -0.15\Psi_1$, for all cases investigated.

The dimensionless version of Equation 16 viscosity is

$$\eta^* = \eta_\infty^* + (\eta_0^* - \eta_\infty^*)[1 + (\mathrm{We}\,\dot{\gamma}^*)^a]^{(n-1)/a} \tag{17}$$

where

$$\eta_0^* \equiv \eta_0/\eta_c, \qquad \eta_\infty^* \equiv \eta_\infty/\eta_c, \qquad \mathrm{We} \equiv \lambda\dot{\gamma}_c, \qquad \dot{\gamma}^* \equiv \dot{\gamma}/\dot{\gamma}_c \tag{18}$$

The Deborah numbers are defined as

$$\mathrm{De}_1 = \frac{\Psi_1\dot{\gamma}_c}{\eta_c}; \qquad \mathrm{De}_2 = -\frac{\Psi_2\dot{\gamma}_c}{\eta_c} \tag{19}$$

The dimensionless first and second normal stress coefficients are given by

$$\Psi_1^* = \frac{\mathrm{De}_1}{\mathrm{Re}}; \qquad \Psi_2^* = \frac{\mathrm{De}_2}{\mathrm{Re}} \tag{20}$$

Boundary conditions and wall quantities

The symmetry of the problem is explored in the sense that only one quarter of the domain is solved; namely, the upper right corner. The appropriate boundary conditions for the problem are shown in Figure 2. The usual impermeability and no-slip conditions are used for the velocity at the walls, and symmetry conditions are imposed at the two other boundaries. The duct is symmetrically heated at the upper and lower walls, while the vertical side walls are adiabatic.

The thermal boundary conditions are investigated at the top and bottom walls; namely, the $H1$ and the $H2$ boundary conditions (Kakaç et al. 1987). For the $H1$ boundary condition, the wall heat flux varies in the crosswise direction [$q_w = q_w(x)$], while the wall temperature is uniform in the crosswise direction, but varies in the downstream direction [$T_w(z)$]. The $H2$ boundary condition is such that the heat flux is uniform throughout the wall surfaces, while the wall temperature varies both in the crosswise and axial directions [$T_w(x, z)$]. It is worth mentioning that the results obtained here for the two boundary conditions were essentially indistinguishable, because the dependence on x of either q_w or T_w, depending on the thermal boundary condition imposed, is for all cases rather weak.

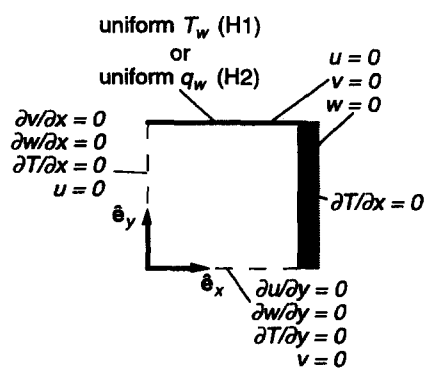

Figure 2 Boundary conditions

The Nusselt number is defined as

$$\mathrm{Nu} = \frac{\bar{q}_w D_h}{k(\bar{T}_w - T_b)} \tag{21}$$

where $\bar{T}_w$ is the mean temperature at the wall, given by

$$\bar{T}_w = \frac{2}{B}\int_0^{B/2} T_w\,\mathrm{d}x \tag{22}$$

and $\bar{q}_w$ is the mean wall heat flux, defined as

$$\bar{q}_w = \frac{2}{B}\int_0^{B/2} q_w\,\mathrm{d}x \tag{23}$$

Clearly, $\bar{T}_w$ reduces to T_w for the $H1$ thermal boundary condition; whereas, $\bar{q}_w$ reduces to q_w for the $H2$ thermal boundary condition.

Numerical solution

Equations 5–9, together with the appropriate boundary conditions, are solved numerically via a finite-volume technique (Patankar 1980). The SIMPLE algorithm is adopted to handle the coupling of the momentum and continuity equations; whereas, the line-by-line Thomas algorithm is used to solve the discretized equations.

Extensive mesh tests showed that uniform grids performed better than nonuniform ones. The meshes employed are: 22×22 for $\alpha = 1$; 24×18 for $\alpha = 2$; and 24×16 for $\alpha = 4$.

For Newtonian fluids, it is easier to assess the accuracy of the solutions obtained with a given mesh. This is so, because exact values of the Nusselt numbers Nu and of the product between friction factor and Reynolds number f Re are available in the literature (e.g., Kakaç et al. 1987). For these Newtonian cases, errors within $\simeq 1\%$ are typically obtained for Nu and f Re with the meshes employed (Table 1). Refining the meshes further does not change the accuracy of the results obtained.

For the non-Newtonian cases, no exact results are available. Therefore, for comparison purposes, results are obtained with finer meshes (32×32 for $\alpha = 1$; 40×26 for $\alpha = 2$; and 42×26 for $\alpha = 4$) for some representative cases. In Table 2, these results are presented and compared with those obtained with the meshes employed.

In Table 2, $\Delta\psi \equiv \psi_{\max} - \psi_{\min}$ is a quantity related to the intensity of the secondary flow, which is defined later in the

Table 1 Mesh tests: Newtonian fluids

α	Mesh	Nu*	Nu_{num}	f Re*	$f\mathrm{Re}_{num}$
1	22×22	4.12	4.10	56.92	56.77
2	24×18	5.20	5.24	62.23	62.00
4	24×16	6.20	6.32	72.94	72.61
1	36×36	4.12	4.10	56.92	56.86
2	42×30	5.20	5.24	62.23	62.13
4	42×26	6.20	6.31	72.94	72.83

*Obtained from Kakaç et al. (1987).

Table 2 Mesh tests: non-Newtonian fluids

α	Mesh	Re	Ψ_2^*	$\Delta\psi$, kg/ms	Nu_{num}
1	22 × 22	330	3.1×10^{-5}	1.48×10^{-3}	8.98
1	36 × 36	330	3.1×10^{-5}	1.50×10^{-3}	8.98
2	24 × 18	260	7.0×10^{-5}	2.09×10^{-3}	12.79
2	40 × 26	260	7.0×10^{-5}	2.10×10^{-3}	12.78
4	24 × 16	193	1.9×10^{-4}	1.87×10^{-3}	10.88
4	42 × 26	193	1.9×10^{-4}	1.91×10^{-3}	10.86

results section. It can be seen that, for $(\psi_{max} - \psi_{min})$ values, the percentage deviations are of the order of 1–1.5%; whereas, for Nu values, the agreement is within 0.2%.

Some difficulties in convergence are caused by the highly nonlinear nature of the governing equations. To overcome these problems and obtain a converged solution, a 0th order continuation procedure in Ψ_2 is employed, starting from the solution for the Newtonian case. Convergence is verified by means of two different methods: (1) evaluation of normalized residuals of the x- and y-momentum equations; and (2) evaluation of an overall heat balance, which should tend to zero as the converged solution is approached.

Results and discussion

For all cases investigated, the friction factor was found to be essentially unaffected by the secondary flows. This finding is in agreement with the observations of a number of researchers (e.g., Mena et al. 1978; Hartnett and Kostic 1985; Hartnett 1992).

It is interesting to analyze the present problem by means of two different approaches: (1) by investigating the effects of geometry and elasticity for a given fluid; and (2) by investigating the effects of the different dimensionless parameters that appear in the above problem formulation. In the present research, both approaches are adopted.

The conclusions obtained with the first approach (the *single-fluid analysis*) are directly applicable to engineering situations for the fluid under investigation, but it is generally not possible to draw conclusions for other fluids, not even for those of same qualitative mechanical behavior. Therefore, generality is lost. When this approach is adopted, the values of the parameters appearing in Equation 16 are held fixed.

The second approach (the *dimensionless analysis*) gives the relative importance of each dimensionless parameter, which allows a better understanding of the physics involved. With this information, it is possible to make predictions for any fluid behaving according to the constitutive equation employed, as long as the values of the related dimensionless parameters are kept within the ranges investigated. However, varying one dimensionless parameter, while maintaining all others fixed, generally means that a different fluid corresponds to each value of the varying parameter. Therefore, for the flow of a given fluid, it may not be simple to extract engineering predictions from results presented in terms of dimensionless parameters. For the analysis performed according to the second approach, the dimensionless viscosity parameters appearing in equation 17 are held fixed.

Single fluid analysis

In this analysis, the viscosity function is given by equation (16). To allow comparisons with available experimental results, the values of the parameters appearing in this equation are taken so as to fit the experimental data of a polyacrylamide solution employed in the experiments reported by Hartnett and Kostic (1985). These values are: $\eta_0 = 0.282$ Pa.s, $\eta_\infty = 3.85 \times 10^{-3}$ Pa.s, $\lambda = 4.74$ s, $n = 0.494$ and $a = 0.942$.

For a single-fluid analysis, the characteristic velocity is chosen to be the mean axial velocity:

$$v_c \equiv \overline{w} \tag{24}$$

and the $H1$ thermal boundary condition is imposed at the top and bottom walls.

Some typical flow patterns are shown in Figure 3–5 for ducts with aspect ratios $\alpha = 1$, 2 and 4; whereas, the other parameters were kept at Re = 690, Pr = 150, $\Psi_2^* = 3.5 \times 10^{-4}$, and $\Psi_1^* = 2.33 \times 10^{-3}$.

The shapes of streamlines are in agreement with those reported by Townsend et al. (1976) and by Gervang and Larsen (1991). It is noted that, as the aspect ratio is increased, the negative vortex becomes smaller in size; whereas, the positive vortex increases to occupy almost all the domain. When Ψ_2^* is increased, the streamline shapes remain unchanged, but the vortex intensity increases.

Hartnett and Kostic (1985) obtained experimental heat transfer results for developing flow of a viscoelastic liquid in a 2×1 rectangular duct. They observed that Nu values for non-Newtonian fluids are larger than for Newtonian fluids. This trend is also observed in this work, and, for some of the cases investigated, the percentage heat transfer enhancements predicted with the present analysis are of the same order of magnitude as those reported by Hartnett and Kostic. However, a quantitative comparison is not possible, because Hartnett and Kostic do not report normal stress coefficient data for the fluid investigated in their experiments.

The following results illustrate how the Nusselt number Nu and the intensity of the secondary flow vary with (1) the Reynolds number, Re; (2) the aspect ratio α; and (3) the first and second normal stress coefficients Ψ_1^* and Ψ_2^*, respectively. It is worth noting that, for a fluid with constant normal stress coefficients, varying Ψ_1^* and Ψ_2^* is possible by varying the hydraulic diameter. Alternatively, we can think of a fixed hydraulic diameter and a hypothetical fluid whose normal stress coefficients can be varied independently of its other material functions. Therefore, Ψ_1^* and Ψ_2^* are dimensionless parameters related to the fluid elasticity for a given duct.

The secondary flow intensity is well quantified by the difference between the extreme values of the stream function, $\psi_{max} - \psi_{min}$. The quantity ψ_{max} is the maximum value of the stream function, which occurs at the "positive" vortex; whereas, ψ_{min} is the minimum value, occurring at the "negative" vortex.

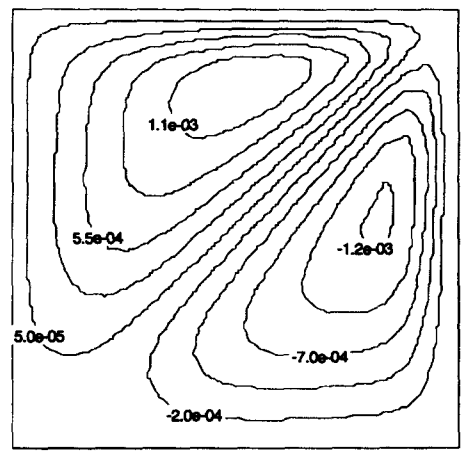

Figure 3 Streamlines for $\alpha = 1$

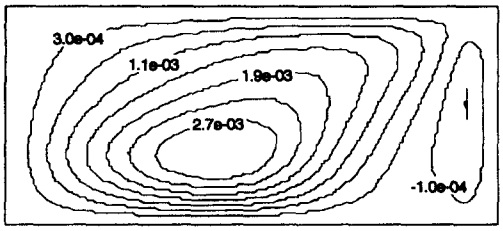

Figure 4 Streamlines for $\alpha = 2$

In Figures 6–9, *Nu* and $(\psi_{max} - \psi_{min})$ are given as functions of Ψ_2^*, for four different Reynolds numbers. Results in Figures 6 and 7 pertain to $\alpha = 1$; whereas, in Figures 8, and 9, the results are for $\alpha = 2$. The first comment about these results is that the qualitative behavior is nearly the same for both aspect ratios.

Comparisons between Newtonian (low Ψ_2^*s) and non-Newtonian values of the Nusselt number are provided in Figures 6 and 8. It can be readily seen that non-Newtonian *Nu* values are much larger. Also, it can be verified that the existence of secondary flows is responsible for the observed heat transfer enhancement, by noting that the Nu curves (Figures 6 and 8) have the same qualitative behavior as the $\Delta\psi \equiv (\psi_{max} - \psi_{min})$ curves (Figures 7 and 9).

For $\Psi_1^* = \Psi_2^* = 0$, (i.e., zero normal stress differences and, hence, no secondary flows) and $\eta(\dot{\gamma})$ (i.e., a shear rate dependent viscosity), Nu is just a little larger (less than 5%) than for the corresponding Newtonian cases. On the other hand, the following can be seen.

(1) For $\alpha = 1$ and Ψ_2^* varying in the range $3 \times 10^{-6} - 1.5 \times 10^{-3}$, the corresponding Nu increment is from 6 to 275%.
(2) For $\alpha = 2$ and Ψ_2^* varying in the range $7 \times 10^{-6} - 3.5 \times 10^{-3}$, the corresponding Nu increment is from 38 to 230%.
(3) For $\alpha = 4$ and Ψ_2^* varying in the range $1 \times 10^{-5} - 1 \times 10^{-2}$, the corresponding Nu increment is from 33 to 130%.

Thus, it can be concluded that the effect of a shear-thinning viscosity on heat transfer enhancement is typically negligible when compared with the secondary flow effect.

Interesting trends can be observed in Figures 6–9. The secondary flow intensity $(\psi_{max} - \psi_{min})$ increases with Ψ_2^* up to a certain value, and from that point on, it starts decreasing monotonically with Ψ_2^*. Therefore, the curves for $(\psi_{max} - \psi_{min})$ present a maximum. It seems that similar trends would be observed in the Nu curves, which is reasonable to expect, but many of the maxima would occur outside the range shown in Figures 6 and 8. Moreover, Figures 7 and 9 show that, in most cases, larger maximum values of $(\psi_{max} - \psi_{min})$ are reached for the lower Re curves.

It is perhaps worth recalling at this point that Nu is a constant, independent of Re, when the fluid is Newtonian, regardless the intensity of the *axial* flow. Therefore, it is readily seen that the non-Newtonian effect on heat transfer is very strong.

There are two important and opposite forces that affect vortex intensity. One is the elastic force, due to the normal stress imbalance Ψ_1^*, and the other is the shear force. The shear force always act against the motion and increases at higher and higher rates as the vortex intensity increases. The elastic force increases

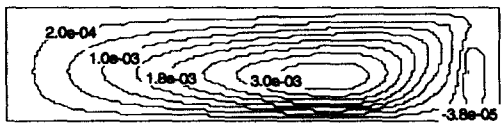

Figure 5 Streamlines for $\alpha = 4$

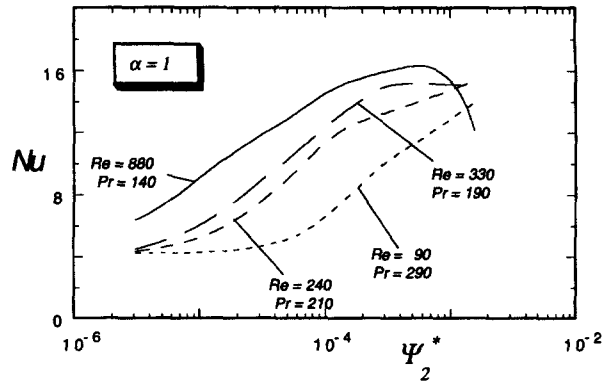

Figure 6 $Nu \times \Psi_2^*$ for $\alpha = 1, 2, 3$

with Ψ_2^* up to a certain point, when the Ψ_1^* effect takes over. Then, it reaches a maximum and decreases thenceforward. Townsend et al. (1976) observed that the effect of Ψ_1 is opposite that of Ψ_2, that is, vortex intensity tends to decrease as Ψ_1 is increased. The effect of Ψ_1 is milder than that of Ψ_2 and is discussed further later in this section.

In this manner, when both Re and Ψ_2^* are small, the secondary flows are weak, and the viscous action does not play a significant role. Therefore, a monotonic increase of Nu and $(\psi_{max} - \psi_{min})$ with these two parameters is observed, when they are both relatively small. As Re (or Ψ_2^*, up to a certain value) is increased, however, the secondary flow gets stronger, and the viscous (shear) force becomes more and more important. Therefore, the slopes of the curves in Figures 6–9 decrease with Ψ_2^*. Furthermore, it starts decreasing earlier for higher Re because vortex intensity is higher for a given value of Ψ_2^*.

It is interesting to note that the maxima occur at somewhat higher Ψ_2^* for the Nu curves, as compared to the corresponding $(\psi_{max} - \psi_{min})$ curves. This is probably due to mild changes in the flow pattern, as the secondary flow intensity varies with Ψ_2^*.

The maximum value of $(\psi_{max} - \psi_{min})$ decreases as Re is increased, because the transversal components of velocity become negligible when compared with the axial component. One exception is observed by the curve for Re = 130 in Figure 9. It seems that in this case, the elastic force starts decreasing due to the Ψ_1^* effect before a high enough secondary flow intensity is achieved to invoke significant viscous action.

As just mentioned above, increasing the first normal stress coefficient, Ψ_1^*, tends to decrease the driving elastic force. Actually, this fact was used above to explain certain trends. To understand better the influence of Ψ_1^*, some extra cases were

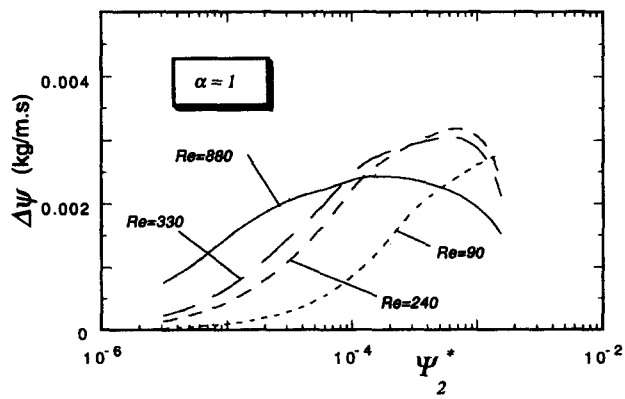

Figure 7 $(\psi_{max} - \psi_{min}) \times \Psi_2^*$ for $\alpha = 1, 2, 4$

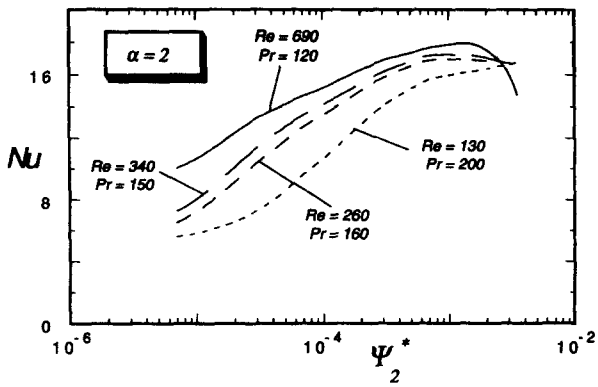

Figure 8 $Nu \times \Psi_2^*$ for $\alpha = 1$

investigated in which Ψ_1^* and Ψ_2^* were decoupled. The results obtained are shown in Table 3. It becomes clear from these results that increasing Ψ_1^* inhibits the secondary flows (and, hence, heat transfer), especially for low Re and high Ψ_2^*.

Dimensionless analysis

In this type of analysis, the dimensionless parameters appearing in the dimensionless viscosity function, (Equation 17), are held fixed at $\eta_0^* = 26.36$, $\eta_\infty^* = 0.36$, We = 1500, $n = 0.494$, and $a = 0.942$. The characteristic velocity is chosen to be

$$v_c \equiv -\frac{\partial p}{\partial z}\frac{D_h^2}{\eta_c} \tag{25}$$

and the $H2$ heat boundary condition is imposed at the top and bottom walls. Moreover, for all cases, the Prandtl number is taken as Pr = 70.

Figure 10 illustrates how Nu varies with Ψ_2^* (or fluid elasticity), for $Re = 2.5 \times 10^4$ and 2.5×10^5 and for three different aspect ratios. The corresponding values of $(\psi_{max} - \psi_{min})$ are shown in Figure 11.

It is noted from these figures that, for small values of Ψ_2^* (or low elastic effects), Nu is larger for larger aspect ratios, as occurs for Newtonian flows. In the high Ψ_2^* range, however, a different trend is observed. The Nusselt number increases as the aspect ratio is increased from $\alpha = 1$ to $\alpha = 2$ but then decreases when the aspect ratio is further increased to $\alpha = 4$. These results imply that, for given values of Ψ_1^* and Ψ_2^* and a given Re, there is a critical aspect ratio that corresponds to maximum heat transfer.

Table 3 Effect of Ψ_1^* for $\alpha = 2$

Re	Pr	Ψ_2^*	Ψ_1^*	Nu	$\Delta\psi$, kg/ms
340	150	7.0×10^{-5}	0.	14.83	3.26×10^{-3}
340	150	7.0×10^{-5}	4.63×10^{-4}	14.70	3.15×10^{-3}
260	160	7.0×10^{-5}	0.	12.84	2.12×10^{-3}
260	160	7.0×10^{-5}	4.63×10^{-4}	12.79	2.09×10^{-3}
260	160	3.5×10^{-4}	10^{-2}	20.81	4.77×10^{-3}
260	160	3.5×10^{-4}	2.31×10^{-2}	16.67	2.70×10^{-3}

The trend described above can be explained as follows. For low values of Ψ_2^*, secondary flows are weak for all aspect ratios, and the Nu behavior is essentially the same as for the Newtonian case. That is, Nu is a monotonically increasing function of α, because, as the heated walls approach each other (with increasing α), the fluid bulk temperature is increased, which causes $\overline{T}_w - T_b$ to decrease. Because the heat flux is constant, Nu must increase for the Newtonian and low Ψ_2^* cases.

As Ψ_2^* is increased, however, the secondary flow gets more intense, becoming responsible for a large (convective) portion of the total heat transfer. However, as the heated plates get close together, a viscous resistance to the secondary flow comes into play, causing the intensity of the vortices (and, hence, heat transfer) to decrease.

It is also seen in Figures 10 and 11 that $(\psi_{max} - \psi_{min})$ decreases in the range of higher values of Ψ_2^*. This indicates that the elastic force that drives the secondary flow decreases after some critical value of Ψ_2^*, or else, a monotonically increasing or at most asymptotic behavior would be expected. The reason for this is related to the first normal stress coefficient, Ψ_1^*. Because Ψ_1^* and Ψ_2^* are proportional to each other, Ψ_1^* is also large in the high Ψ_2^* range. As discussed earlier, the driving elastic force decreases as Ψ_1^* is increased, which explains the observed trend. Because of slight flow pattern changes due to secondary flow intensity changes, the maxima occur at somewhat higher Ψ_2^* for the Nu curves, as compared to the corresponding $(\psi_{max} - \psi_{min})$ curves.

Conclusions

The flow of non-Newtonian fluids inside rectangular ducts has been investigated. The governing differential equations of mass, momentum, and energy were solved numerically by a finite volume technique. The viscoelastic behavior of the flowing fluid was described via the Criminale–Ericksen–Filbey (CEF) constitutive equation.

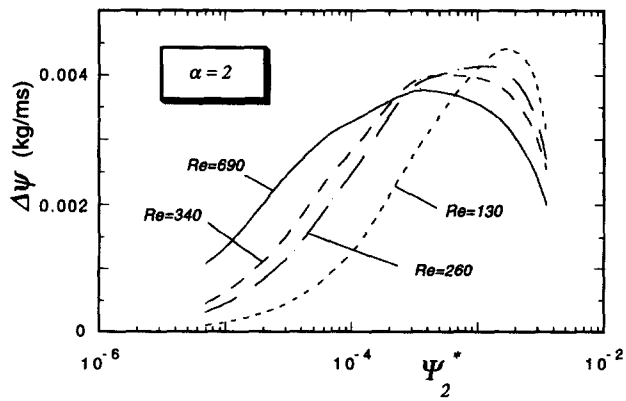

Figure 9 $(\psi_{max} - \psi_{min}) \times \Psi_2^*$ for $\alpha = 1$

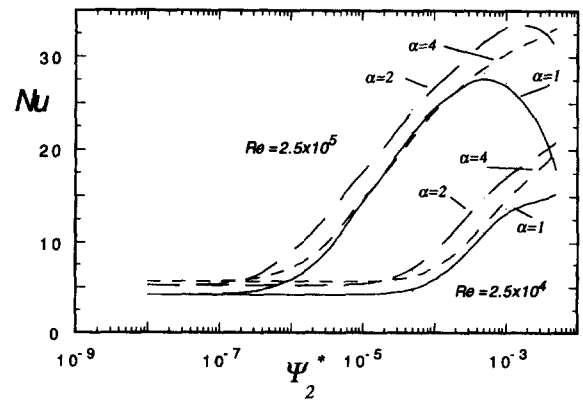

Figure 10 $Nu \times \Psi_2^*$ for $\alpha = 2$

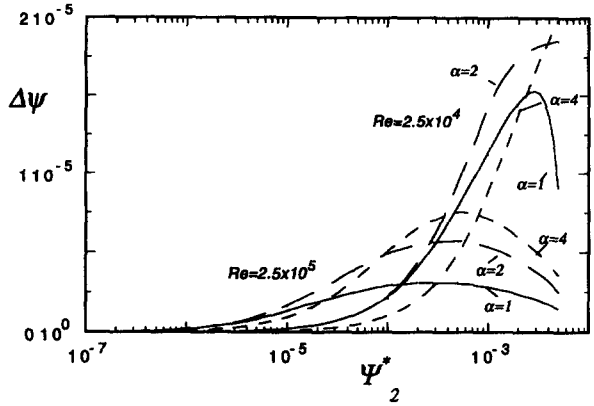

Figure 11 $(\psi_{max} - \psi_{min}) \times \Psi_2^*$ for $\alpha = 2$

Secondary flows are caused by elastic forces related to the second normal stress difference. Other parameters influence secondary flows, such as the aspect ratio, the Reynolds number, and the first normal stress difference. However, the second normal stress difference plays the dominant role.

The dependence of secondary flow intensity and heat transfer on these parameters was investigated. It was found that heat transfer is strongly enhanced by secondary flows, Nusselt numbers reaching values as large as three times those for corresponding Newtonian ones.

Two different analyses were performed, which allowed a more comprehensive study of the physical situation. The single-fluid analysis is the most common in the rheology literature and provides information related to a given fluid. The dimensionless analysis can show the relative importance of the different flow phenomena.

Perhaps the most interesting finding is related to maximum heat transfer that was shown to occur for some combinations of parameters. This implies that there are optimal aspect ratios and Reynolds numbers in the sense of maximum heat transfer, which depend on the fluid's mechanical behavior. This fact might be explored in future thermal deigns of certain industrial processes.

Acknowledgments

The authors are indebted to Angela O. Nieckele for kindly sharing with them her expertise on the finite volume method. The authors wish to express their gratitude to CNPq (Brazilian Council for the National Scientific and Technological Development) for the fellowships provided during the course of the present research. This work was supported by the Ministério de Ciência e Tecnologia da Presidência da República (MCT/PR) (Ministry of Science and Technology of the Brazilian Federal Government).

References

Bird, R. B., Armstrong, R. C. and Hassager, O. 1987. *Dynamics of Polymeric Liquids*. Vol. 1, 2nd ed., Wiley, New York

Chandrupatla, A. R. and Sastri, V. M. K. 1977. Laminar forced convection heat transfer of a non-Newtonian fluid in a square duct. *Int. J. Heat Mass Transfer*, **20**, 1315–1324

Dunwoody, N. T. and Hamill, T. A. 1980. Forced convection in lineal flow of non-Newtonian fluids through rectangular channels. *Int. J. Heat Mass Transfer*, **23**, 943–949

Gao, S. X., and Hartnett, J. P. 1996. Heat transfer behavior of Reiner–Rivlin fluids in rectangular ducts. *Int. J. Heat Mass Transfer*, **39**, 1317–1324

Gervang, B. and Larsen, P. S. 1991. Secondary flows in straight ducts of rectangular cross section, *J. Non-Newtonian Fluid Mech.*, **39**, 217–237

Gringrich, W. K., Cho, Y. I. and Shyy, W. 1992. Effects of shear thinning on laminar heat transfer behavior in rectangular duct. *Int. J. Heat Mass Transfer* **35**, 2823–2836

Hartnett, J. P. 1992. Viscoelastic fluids: A new challenge in heat transfer. *J. Heat Transfer*, **114**, 296–303

Hartnett, J. P. and Kostic, M. 1985. Heat transfer to a viscoelastic fluid in laminar flow through a rectangular channel. *Int. J. Heat Mass Transfer*, **28**, 1147–1155

Kakaç, S., Shah, R. K. and Aung, W. 1987. *Handbook of Single-Phase Convective Heat Transfer*. Wiley, New York, 3.8–3.52

Kostic, M. 1994. On turbulent drag and heat transfer reduction phenomena and laminar heat transfer enhancement in non-circular duct flow of certain non-Newtonian fluids. *Int. J. Heat Mass Transfer*, **37**, 133–147

Mena, B., Best, G., Bautista, P. and Sanchez, T. 1978. Heat transfer in non-Newtonian flow through pipes. *Rheol. Acta*, **17**, 454–457

Naccache, M. F. 1993. Mixed convection in the flow of viscoelastic fluids through rectangular ducts. Ph.D. thesis, Department of Mechanical Engineering, Pontifícia Universidade Católicfa, Rio de Janeiro, Brazil (in Portuguese)

Naccache, M. F. and Souza Mendes, P. R. 1992. Heat transfer in non-Newtonian flows inside rectangular ducts. *Proc. 4th Brazilian Thermal Science Meeting*, Rio de Janeiro, Brazil, 573–576

Patankar, S. V. 1980. *Numerical Heat Transfer and Fluid Flow*. Hemisphere, Bristol, PA

Townsend, P., Walters, K. and Waterhouse, W. M. 1976. Secondary flows in pipes of square cross-section and the measurement of the second normal stress difference. *J. Non-Newtonian Fluid Mech.* **1**, 107–123